Final Technical Report
(Revised)

DOE Award Grant Number: DOE-FG02-ER46535

University of California, Santa Barbara (UCSB)

Project Title: Charge Recombination, Transport Dynamics, and Interfacial Effects in Organic Solar Cells

Principal Investigator: Alan J. Heeger
Co-PIs: Guillermo C. Bazan, Thuc-Quyen Nguyen, Fred Wudl

Date of Report: February 12, 2015

Note: No distribution limitations; no patentable material and no protected data.

1. Executive Summary of Results (#DE-FG02-08ER46535)

The need for renewable sources of energy is well known. Conversion of sunlight to electricity using solar cells is one of the most important opportunities for creating renewable energy sources. The research carried out under *DE-FG02-08ER46535* focused on the science and technology of "Plastic" solar cells comprised of organic (i.e. carbon based) semiconductors. The Bulk Heterojunction concept involves a phase separated blend of two organic semiconductors each with dimensions in the nano-meter length scale --- one a material that functions as a donor for electrons and the other a material that functions as an acceptor for electrons. The nano-scale inter-penetrating network concept for "Plastic" solar cells was created at UC Santa Barbara. A simple measure of the impact of this concept can be obtained from a Google search which gives 244,000 "hits" for the Bulk Heterojunction solar cell.

Research funded through this program focused on four major areas:

1. Interfacial effects in organic photovoltaics,
2. Charge transfer and photogeneration of mobile charge carriers in organic photovoltaics,
3. Transport and recombination of the photogenerated charge carriers in organic photovoltaics,
4. Synthesis of novel organic semiconducting polymers and semiconducting small molecules, including conjugated polyelectrolytes.

Following the discovery of ultrafast charge transfer at UC Santa Barbara in 1992, the nano-organic (Bulk Heterojunction) concept was formulated. The need for a morphology comprising two interpenetrating bicontinuous networks was clear: one network to carry the photogenerated electrons (negative charge) to the cathode and one network to carry the photo-generated holes (positive charge) to the anode. This remarkable self-assembled network morphology has now been established using Transmission electron Microscopy (TEM) either in the Phase Contrast mode or via TEM-Tomography.

The steps involved in delivering power from a solar cell to an external circuit are the following:

- Photo-excitation of the donor (or the acceptor).
- Charge transfer with holes in the donor domain and electrons in the acceptor domain.
- Sweep-out to electrodes prior to recombination by the internal electric field.
- Energy delivered to the external circuit

Each of these four steps was studied in detail using a wide variety of organic semiconductors with different molecular structures. This UC Santa Barbara group was the first to clarify the origin and the mechanism involved in the ultrafast charge transfer process. The ultrafast charge transfer (time scale approximately 100 times faster than the first step in the photo-synthesis of green plants) is the fundamental reason for the potential for high power conversion efficiency of sunlight to electricity from plastic solar cells. The UCSB group was the first to emphasize, clarify and demonstrate the need for sweep-out to electrodes prior to recombination by the internal electric field. The UCSB group was the first to synthesize small molecule organic semiconductors capable of high power conversion efficiencies.

The results of this research were published in high impact peer-reviewed journals. Our published papers (40 in number) provide answers to fundamental questions that have been heavily discussed and debated in the field of Bulk Heterojunction Solar Cells; scientific questions that must be resolved before this technology can be ready for commercialization in large scale for production of renewable energy. Of the forty publications listed, nineteen were co-authored by two or more of the PIs, consistent with the multi-investigator approach described in the original proposal.

The specific advantages of this "plastic" solar cell technology are the following:

a. Manufacturing by low-cost printing technology using soluble organic semiconductors; this approach can be implemented in large scale by roll-to-roll printing on plastic substrates.
b. Low energy cost in manufacturing; all steps carried out at room temperature (approx. a factor of ten less than the use of Silicon which requires high temperature processing).
c. Low carbon footprint
d. Lightweight, flexible and rugged

"Plastic" Solar Cells

Low $ cost manufacturing
Low energy cost manufacturing
Low carbon "footprint" manufacturing

Technology	Energy for production ($MJ.Wp^{-1}$)	CO_2 footprint ($gr.CO_2\text{-}eq.Wp^{-1}$)	Energy payback time (years)
mc-Si	24.9	1293	1.95
CdTe	9.5	542	0.75
CIS	34.6	2231	2.71
Flex OPV	2.4	132	0.19

A. L. Roes *et al, Progress in Photovoltaics* 17, 372 (2009)

Because of the resolution of many scientific issues, a significant fraction of which were addressed in the research results of *DE-FG02-08ER46535*, the power conversion efficiencies are improving at an ever increasing rate. During the funding period of *DE-FG02-08ER46535,* the power conversion efficiencies of plastic solar cells improved from just a few per cent to values greater than 11% with contributions from our group and from researchers all over the world.

2. Comparison of actual accomplishments with the goals and objectives of the project

As demonstrated by the publication list in Section 5, the actual accomplishments were indeed consistent with the goals of the project. The published results demonstrated major progress in each of the four focus areas:

Interfacial effects in organic photovoltaics (OPVs),
Charge transfer and photogeneration of mobile charge carriers,
Transport and recombination of the photogenerated charge carriers in OPVs,
Synthesis of novel semiconducting polymers and small molecules, including conjugated polyelectrolytes (CPEs).

Some Highlights are given in Section 3. Due to space limitations, it is not possible to review all the research output. Complete details can be found in the published work.

3. Highlights of project activities for the entire period of funding

A. Period 2009 – 2011

Accomplishments during the period 2009 -2011:

a) Understanding charge carrier dynamics and charge recombination in BHJ solar cells through new experimental methods.

b) Understanding charge recombination mechanism in BHJ solar cells.

c) Probing the effect of film morphology and phase separation on the charge generation, transport, and collection using scanning probe microscopy.

d) Improving the open-circuit voltage and fill factor and hence the device efficiency by introducing an interlayer between the active layer and the Al cathode.

1. Photoexcitation and charge transfer in BHJs

Understanding charge generation dynamics in BHJ solar cells is important. In a recent paper to the Journal of the American Chemical Society, N. Banerji, S.R. Cowan, and A.J. Heeger,[i] *the nature and time evolution of the primary excitations in the pristine conjugated polymer, PCDTBT*, are investigated by femtosecond-resolved fluorescence up-conversion spectroscopy. PCDTBT is poly[[9-

(1-octylnonyl)-9H-carbazole-2,7-diyl]-2,5-thiophenediyl-2,1,3-benzothiadiazole-4,7-diyl-2,5-thiophenediyl]. The extensive study includes data from PCDTBT thin film and from PCDTBT in chlorobenzene solution, compares the fluorescence dynamics for several excitation and emission wavelengths, and is complemented by polarization-sensitive measurements. The results are consistent with the photogeneration of mobile electrons and holes by interband $\pi-\pi^*$ transitions, which then self-localize within about 100 fs and evolve to a bound singlet exciton state in less than 1 ps. The excitons subsequently undergo successive migrations to lower energy localized states, which exist as a result of disorder. In parallel, there is also slow conformational relaxation of the polymer backbone. While the initial self-localization occurs faster than the time resolution of our experiment, the exciton formation and conformational changes lead to a progressive relaxation of the inhomogeneously broadened emission spectrum with time constants ranging from about 500 fs to tens of picoseconds.

The time scales for the relaxation processes in pristine PCDTBT are compared to the time scale (<0.2 ps) previously reported for photo-induced charge transfer in phase-separated PCDTBT:fullerene blends.[ii] We note that exciton formation and migration in PCDTBT occur at times much longer than the ultrafast photoinduced electron transfer time in PCDTBT:fullerene blends. This disparity in time scales is not consistent with the commonly proposed idea that photoinduced charge separation occurs after diffusion of the polymer exciton to a fullerene interface. We therefore must consider alternative mechanisms that are consistent with ultrafast charge separation before localization of the primary excitation to form a bound exciton, as outlined in Figure 1.

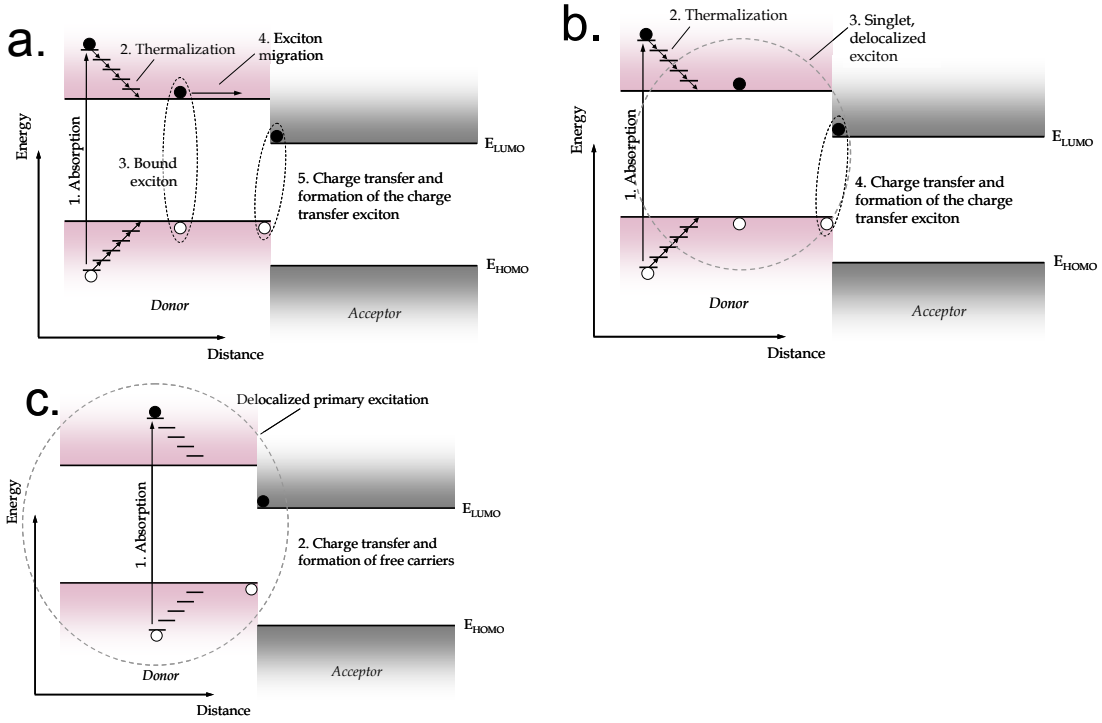

Figure 1. Several proposed methods for the formation of mobile carriers from photoexcitation in organic BHJ solar cells: (a) Excitation forms a bound exciton after thermalization to the band edge. Exciton diffuses to a BHJ interface and charge transfers. (b) Primary excitation forms a bound exciton after thermalization to the band edge. Delocalized singlet exciton can sample spatial distances of 1 nm to 10 nm. (c) Primary excitation charge transfers before thermalization to form mobile carriers in less than 1 ps.

2. Charge transport in BHJ materials

Under illumination, excess carriers are created in the polymer and fullerene domains due to photoexcitation and charge transfer. The excess carriers populate the energy states near the band edge. Recombination lifetimes of the charge carriers in the donor and acceptor materials limit the efficient extraction of these carriers to an external circuit. In donor and acceptor materials with low trap density, the recombination lifetime is determined by the density and location of localized states – states deep in the disordered band tails. In materials with high trap densities, recombination lifetimes can become dominated by trapping and recombination.

Once excitation and charge transfer occur, free carriers must be collected at opposite electrodes before they recombine, as temporally resolved in Figure 2 and Figure 3. The interpenetrating bulk heterojunction materials form two-carrier transport paths (networks) back to the anode and cathode. Charge transport has been studied extensively for polymer materials and BHJ solar cells. The fundamental discovery of near 100% internal quantum efficiency by S.H. Park, et al.[1] has lead to fundamental physical insight via the PCDTBT:$PC_{70}BM$ BHJ system.

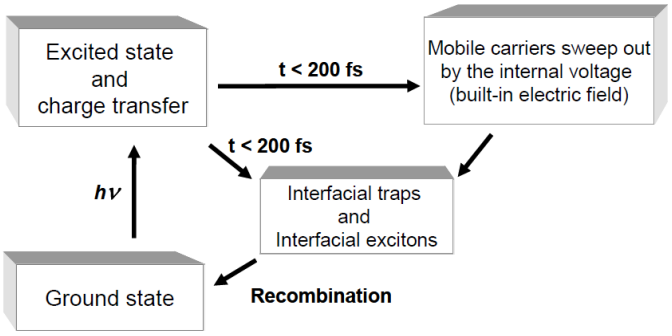

Figure 2. Time dynamics during the operation of the BHJ solar cell. Photoexcitation is followed by ultrafast charge transfer that creates mobile carriers in the donor and acceptor domains. These carriers are subsequently either swept out to the electrodes by the built-in electric field, or they recombine to the ground state. The sweep-out time is less than 1 μs at short circuit where the recombination probability is small. For efficient solar cells, the recombination time must be long compared to the sweep-out time.

Transient photoconductivity measurements carried out on bulk heterojunction (BHJ) solar cells demonstrate the competition between carrier sweep-out by the internal field and the loss of photogenerated carriers by recombination.[iii] The transient photoconductance data in Figure 3 imply the existence of a well-defined internal field; carrier sweep-out is proportional to the magnitude of the internal field and limited by the carrier mobility. At external voltages near open circuit where the internal field approaches zero, the photocurrent decays because of the recombination of photogenerated mobile carriers. Mobility and recombination lifetimes were evaluated for carriers in poly[3-hexylthiophene] (P3HT): [6,6]-phenyl-C61-butyric acid methyl ester ($PC_{60}BM$) and PCDTBT): [6,6]-phenyl-C71-butyric acid methyl ester ($PC_{71}BM$) solar cells.

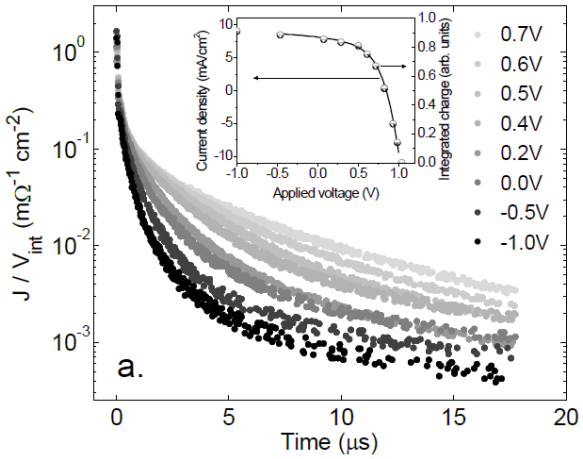

Figure 3. Transient photoconductance versus time for the PCDTBT:$PC_{71}BM$ cell collected at 300 K. Inset: Data points are the integrated charge collection obtained by integrating the unnormalized transient current data for the PCDTBT:$PC_{71}BM$ cell; solid line is the steady-state white light *J-V* curve.

In amorphous organic materials, charge can be thought to be relatively delocalized along the π-conjugated backbone. Conduction between molecules requires tunneling from one molecule to another. This tunneling process is heavily assisted by electron-phonon interactions (hopping transport). An alternate process assumes relatively mobile charge at the band edge and ongoing trapping and de-trapping processes from unfilled states in the band tails.

Optical absorption is influenced by the electron-phonon coupling, the presence of disorder-induced band tail states and excitonic transitions. At the BHJ interface, there is experimental evidence and theoretical expectation that the charge transfer exciton has a smaller binding energy and lower oscillator strength than for bulk excitations because the electron and hole are localized on opposite sides of the interface.

3. Recombination mechanisms via interfaces and defect states

Recombination of excess charge through localized states or trap states occurs radiatively or non-radiatively. In the radiative recombination mechanism, an electron transitioning to a relaxed state releases the transition energy via a photon. This photon can be detected 2via luminescence experiments, although this process is typically thought to inefficient in polymer:fullerene BHJ films. In the non-radiative recombination mechanism, an electron's relaxation is mediated via phonon emission. Carrier densities are not thought to be high enough in these materials to support measurable Auger recombination, where the transition energy is kinetically transferred to a nearby charge carrier, promoting it to a higher energy level. Phonon assisted recombination over a larger energy gap may require higher energy phonons or multiple spatially correlated phonons, and hence these transitions are less likely than lower energy transitions.

In polymer:fullerene BHJs, bimolecular recombination, seen in Figure 4a, is the dominant loss mechanism, as intensively detailed in the literature. Seen in Figure 4b, trap-assisted recombination is suppressed because of the relatively low localized state density and low impurity levels in efficient materials.

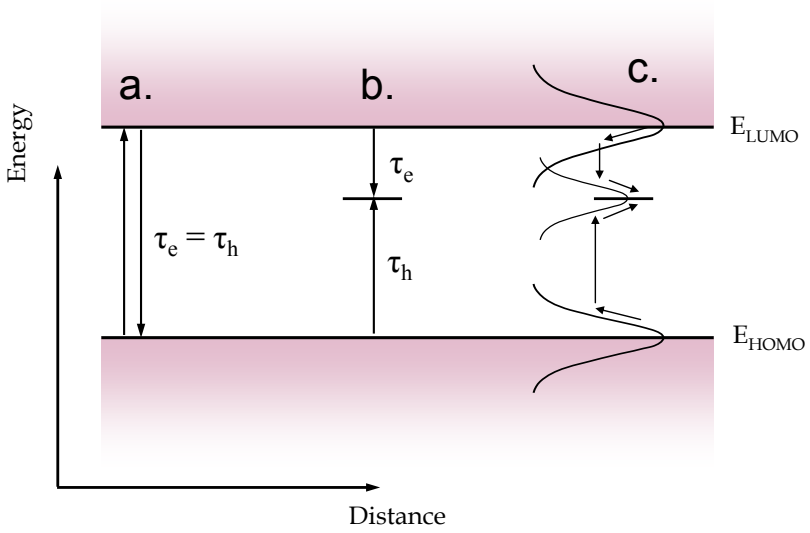

Figure 4. Recombination mechanisms of excess carriers considered in this dissertation: (a) Bimolecular (band-to-band) recombination; (b) Trap-assisted recombination; and (c) the Taylor-Simmons approximation of SRH recombination for disordered materials.

In one of our recent papers,[ii] a clear experimental test is demonstrated which can distinguish between geminate and non-geminate recombination in low mobility semiconductors. Measurements carried out at room temperature and 200 K on BHJ organic solar cells fabricated with two different semiconducting polymers show that neither exhibits significant geminate recombination.

Recombination of photogenerated charge carriers in polymer BHJ solar cells reduces the short circuit current (J_{sc}), the fill factor (FF) and the open-circuit voltage (V_{oc}).[iv] Identifying the mechanism of recombination is, therefore, fundamentally important for increasing the power conversion efficiency. Light intensity and temperature-dependent current-voltage measurements on polymer BHJ cells made from a variety of different semiconducting polymers and fullerenes show that the recombination kinetics are voltage dependent and evolve from first-order dynamics at short circuit to bimolecular recombination at open circuit as a result of increasing the voltage-dependent charge carrier density in the cell. Figure 5(a) illustrates the universality of the bimolecular recombination behavior probed via intensity-dependent V_{oc} measurements. The "missing 0.3 V" inferred from comparison of the band gaps of the BHJ materials and the measured V_{oc} at room-temperature results from the temperature dependence of the quasi-Fermi levels in the polymer and fullerene domains—a conclusion based on the fundamental statistics of fermions. Figure 5(b) illustrates the linear dependence of V_{oc} with temperature in a PCDTBT:$PC_{71}BM$ solar cell.

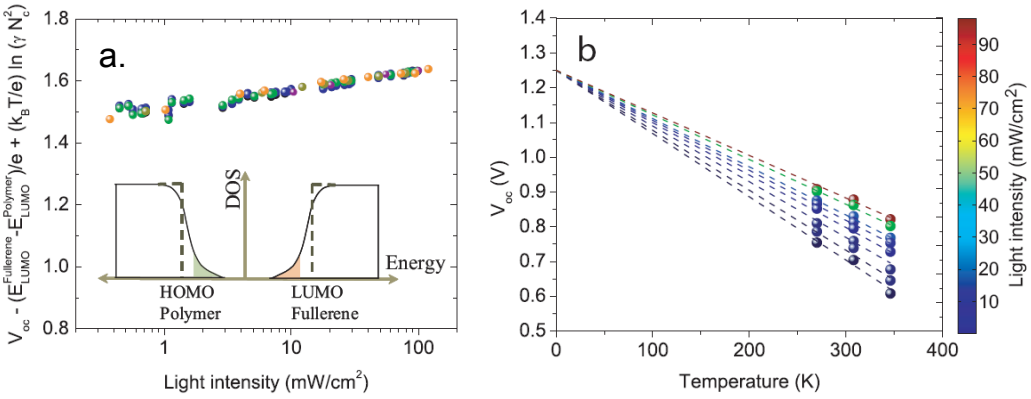

Figure 5. (a) Universal curve showing the incident light intensity dependence of V_{oc} for 7 optimized polymer:fullerene BHJ solar cells. Inset: schematic of the density of states in the band "tails" and the intensity-dependent quasi-Fermi energies at T=0 K as the tails are filled by photo-excited electrons in the fullerene component and holes in the polymer component. At finite temperatures, the quasi-Fermi energies move into the gap. (b) Linear dependence of V_{oc} with temperature in a PCDTBT:$PC_{71}BM$ solar cell.

Small amounts of impurity, even one part in one thousand, in polymer bulk heterojunction solar cells can alter the electronic properties of the device, including reducing the open circuit voltage, the short circuit current and the *FF*. Steady state studies show a dramatic increase in the trap-assisted recombination rate when [6,6]-phenyl C84 butyric acid methyl ester ($PC_{84}BM$) is introduced as a trap site in polymer BHJ solar cells made of a blend of PCDTBT and $PC_{60}BM$, as pictured in Figure 6(a). The trap density-dependent recombination studied here can be described as a combination of bimolecular and Shockley-Read-Hall recombination; the latter is dramatically enhanced by the addition of the $PC_{84}BM$ traps. This study reveals the importance of impurities in limiting the efficiency of organic solar cell devices and gives insight into the mechanism of the trap-induced recombination loss.

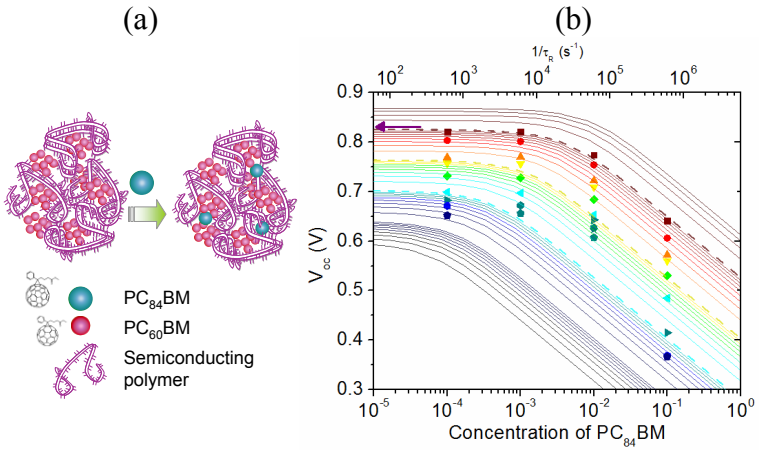

Figure 6. (a) Schematic illustration of the addition of $PC_{84}BM$ in small mass fraction to the polymer bulk-heterojunction solar cell; legend shows the chemical structure of $PC_{84}BM$ and $PC_{60}BM$. (b) Intensity dependent V_{oc} plotted as a function of $PC_{84}BM$ trap concentration (data points, lower x-axis). Bimolecular/SRH recombination model fits to the data (lines, upper x-axis): the trap-assisted recombination rate plotted vs. the generation rate of excitons with color from blue to brown indicating an increase in generation rate. Arrow indicates the V_{oc} at 1 sun for the trap-free PCDTBT:$PC_{60}BM$ solar cell devices. Dotted lines correspond to logarithmic increases in generation rate (G(brown) = 10^{21} cm^{-3} s^{-1}, G(yellow) = 10^{20} cm^{-3} s^{-1}, G(blue) = 10^{19} cm^{-3} s^{-1}).

The trap-assisted recombination rate (proportional to the trap density) and the generation rate (proportional to incident light intensity) control the cross-over regime from bimolecular to trap-assisted recombination, as plotted in data and model in Figure 6(b). Above the cross-over point at low trap densities and high light intensities, the open circuit voltage is relatively unaffected by the density of traps within the BHJ due to disordered band tails or intentionally introduced traps. Below the cross-over point at high trap densities, such as those potentially found in BHJ materials with impurities left over from the synthesis and device processing, recombination through traps becomes the dominant loss mechanism and results in reduction in the V_{oc} under operating illumination levels.

The response of the solar cell to an alternating current (AC) signal provides information on the recombination parameters and is used to investigate the role of traps by W.L. Leong, S. Cowan, and A.J. Heeger.[v] Impedance spectroscopy is a commonly used method of profiling a device's AC response and has been employed extensively in dye-sensitized solar cells to correlate device fabrication techniques and photovoltaic performance. Impedance spectroscopy has only recently been utilized in the characterization of polymer and small molecule BHJ systems.[vi]

In general, impedance spectroscopy utilizes a small amplitude sinusoidal voltage, $V_{AC}(\omega)$, rippled over a constant DC voltage bias, V_{DC}. One measures the AC current response, $i_{AC}(\omega)$, as a function of the angular frequency, ω. The impedance, $Z(\omega)$ is given as $V_{AC}(\omega)/i_{AC}(\omega)$. By modifying the steady state operating parameters (e.g. illumination intensity or V_{DC}) and scanning the frequency ($f = \omega/2\pi$), the change in impedance parameters (resistances, capacitances) can be monitored and interpreted in terms of the physical properties of the BHJ system.

The measured impedance is complex and is represented in terms of magnitude and phase; $Z(\omega) = Z'(\omega) + iZ''(\omega)$, where $Z'(\omega)$ is the real part and $Z''(\omega)$ is the imaginary part of the frequency response of the solar cell. The addition of impurities, which act as traps to mobile carriers, increases both the magnitude and the phase of the measured impedance. Thus, $Z(\omega)$ provides information on the traps and how they hinder the dynamic response of the BHJ material.

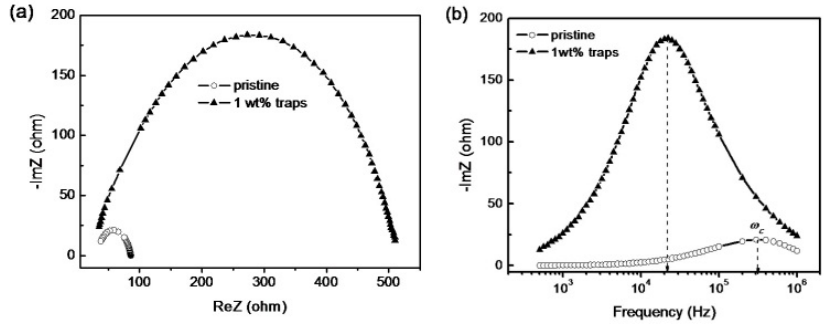

Figure 7. (a) Impedance spectra of Cole-Cole plot and (b) Frequency dependent of imaginary part of the impedance measured for PCDTBT:$PC_{60}BM$ standard cell and device containing 1 wt% of $PC_{84}BM$ traps. The graph is marked to clearly indicate the characteristic frequency ω_c (at Im(Z) is maximum).

As shown above in Figure 7(a) presents the impedance spectra of the PCDTBT:$PC_{60}BM$ solar cells and the corresponding cell with 1 wt% of $PC_{84}BM$ molecules. The data were obtained under 1 sun illumination and at a bias voltage $V_{app} = V_{oc}$. The real part, $Z'(\omega)$ and imaginary part, $Z''(\omega)$ of the complex impedance are plotted (Nyquist plots); all the spectra are characterized by a major arc which is related to the recombination resistance. Qualitatively, the increased magnitude of the real and imaginary components of the impedance in the presence of trap states results from the reduced (trap-limited) carrier mobility. This result correlates well with the steady state measurement of lower J_{sc} in the trap-containing device.

The imaginary part, $Z''(\omega)$, of the complex impedance for both devices are plotted as functions of frequency in Figure 7(b) to clearly show the characteristic frequency ω_c. The characteristic frequency is defined as the frequency at which $Z''(\omega)$ is maximum and is related to the response time or lifetime (τ) of the charge carriers, such that $\tau = \omega_c^{-1}$. The lifetime of charge carriers can also be determined through fitting of the complex impedance spectra by an equivalent RC circuit model. The carrier lifetime increases with the incorporation of traps: $\tau = 0.6$ µs for standard PCDTBT:$PC_{60}BM$ device, whereas $\tau = 7.1$ µs for device containing 1 wt% of $PC_{84}BM$ traps.

4. Conjugated Polyelectrolyte and Oligoelectrolyte Interlayers

According to the equation for solar cell efficiency:

$$\eta = \frac{V_{oc} I_{sc} FF}{P},$$

one must increase I_{sc}, FF and V_{oc} to achieve higher efficiency. The "traditional" strategy for increasing I_{sc} and FF involves choosing materials with higher mobilities and lower band gaps. An alternative approach is to improve the morphology of the BHJ material by altering processing conditions. V_{oc} is roughly determined by the difference between the donor HOMO and acceptor LUMO energy levels, thus, controlling the HOMO of the donor leads to higher V_{oc}. However, other factors are involved, and this simple approach does not always provide a reliable guideline.

Work from our groups[vii] has shown that the V_{oc} of solar cells can be significantly modified upon introduction of a thin conjugated polyelectrolyte (CPE) interlayer between the BHJ active layer and the electron collecting electrode. CPEs are defined for our purpose as polymers having a backbone with a π-delocalized electronic structure and pendant substituents with ionic functionalities.[viii] The properties of these materials in solution and in the solid state are difficult to predict *a priori* from simple molecular structure considerations, since they combine the well-known complexity of polyelectrolytes, for which physicochemical properties depend on variable long-range electrostatic interactions,[ix] with the rigid and highly hydrophobic nature of conjugated polymers. From a practical perspective, incorporation of CPE layers into optoelectronic devices is facilitated by their solubility in highly polar solvents; by alternating deposition of solutions with orthogonal polarities, one can build sophisticated polymer multilayers with little or no disturbance of previously deposited underlayers.[x] Indeed, it has been shown that CPE incorporation leads to improvements in the performance of various types of devices including in organic electronic devices, such as organic light-emitting devices,[xi] thin-film transistors[xii] as well as biological and chemical sensors.[xiii]

Figure 8 shows how a CPE interlayer leads to a 0.15 V increase in the V_{oc} of BHJ solar cells containing the PFO-DBT35 (poly[(9,9-dioctylfluorene)-*co*-(4,7-di-2-thienyl-2,1,3-benzothiadiazole)] with DBT monomer molar ratio of 35%) donor material and PCBM as the acceptor.[vii] Figure 8 also shows the chemical structure of the CPE utilized, namely PF-Br. However, there is no improvement when using the donor polymers P3HT (poly(3-hexylthiophene) or MEH-PPV (poly(2-methoxy-(2'-ethyl-hexoxy)-1,4-phenylenevinylene). Why this difference exists is not particularly understood and will be discussed in more detail below. Examination of *J-V* characteristics of the devices in Figure 8 under dark conditions reveals that there is considerable decrease of the dark currents. Such conditions can lead to increases in V_{oc}.[xiv] Thus, two possible phenomena may be participating: (i) increase of the built-in field as a result of dipole layer formation adjacent to the cathode, as observed in polymer light emitting diodes, and (ii) reduced leakage currents. It is unknown at this point to what extent each phenomenon contributes to the overall increase in performance and to what degree they may be convoluted.

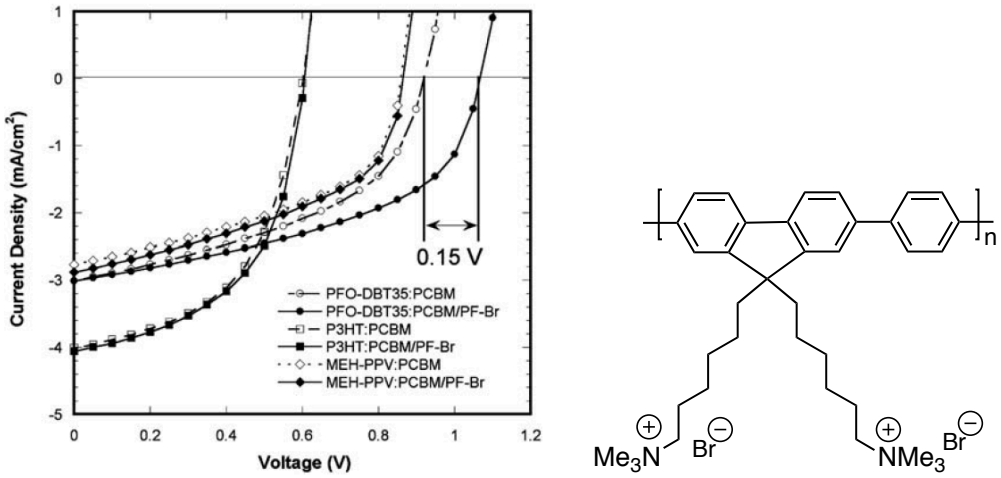

Figure 8. Typical *J–V* characteristics of PFO-DBT35:PCBM, P3HT:PCBM and MEH-PPV:PCBM devices with or without PF-Br cathode interface layer under AM 1.5G illumination. Also shown is the molecular structure of PF-Br.

More recently, work by Kim et al. demonstrated that a different CPE material could be used to increase the V_{oc} of P3HT:PCBM devices by approximately 0.1 V when using an Al electrode. Moreover, it was also demonstrated that the PCE of devices using Cu electrodes can be increased from 0.8 % to 3.4 %. These findings are remarkable from a practical perspective, but also highlight how the interfacial phenomena are acutely dependent on how the CPE self assembles. Thin CPE layers are essential so that the hydrophobic portion of their structure, namely the conjugated backbone, preferentially associates with the BHJ underlayer and thereby provides a driving force for dipole formation by the ionic component.

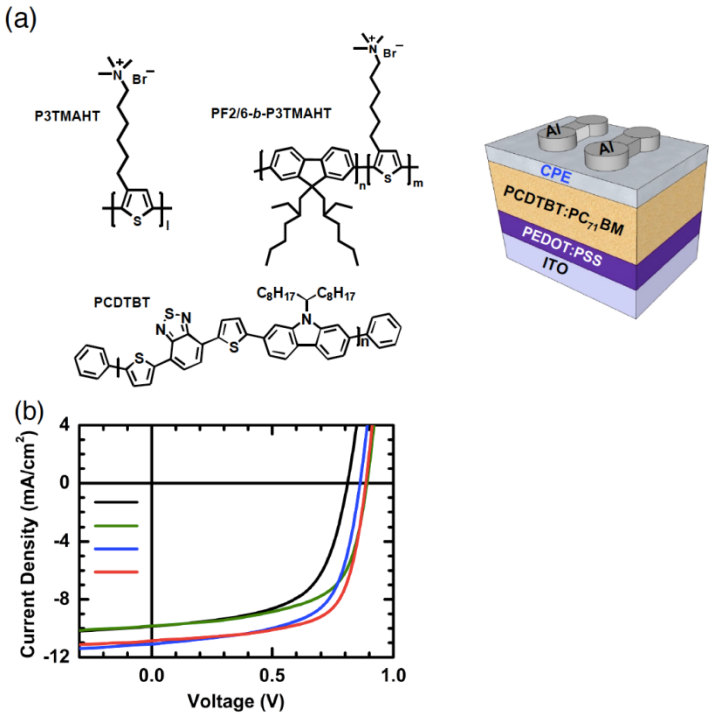

Figure 9. (a) Molecular structures of the materials used for device fabrication. In PF2/6-*b*-P3TMAHT, average numbers of n and m are 16 and 27, respectively. Device configuration for the solar cells used in this study. (b) *J-V* characteristics of PCDTBT:$PC_{71}BM$ devices with no CPE layer (black), with thin P3TMAHT (blue) and PF2/6-*b*-P3TMAHT layers (red) under illumination of an AM 1.5G solar simulator, 100 mW/cm^2. Methanol (green) was spin-cast on top of active layer for comparison.

Unpublished work carried out in our laboratories shows that the CPE approach can also be used for improving high performance devices. Figure 9 (a) above illustrates the materials used in these studies, together with the device test structure. Note that the CPEs include a cationic poly(thiophene) (P3TMAHT) and a block copolymer containing a cationic poly(thiophene) segment (PF2/6-*b*-P3TMAHT). As shown in Figure 9(b) the device efficiency increases from 5 % (black line) to 6.5 % in the case of PF2/6-*b*-P3TMAHT (red line)! It is worth noting that poly(thiophene) is much more commonly understood to be a good hole transport material, instead of an electron carrier, thus the data in Figure 9(b) imply that the HOMO and LUMO levels of the CPE backbone play only a minor role – most of the positive effect likely arises due to interfacial dipoles. Figure 9(b) also reveals an important new remarkabe observation; the simple treatment of the BHJ layer with methanol leads to an increase in V_{oc}. These experiments were carried out as controls since the CPEs are best deposited from this solvent. Furthermore, the improvement appears to be quite general, as determined by a wide range of narrow band gap conjugated polymers tested at UCSB.

BHJ solar cells utilizing oligoelectrolytes as electron transporting layers (ETLs) also show higher efficiencies than those devices without the ETLs (5.2% versus 4.3%), see Figure 10.[xv] Molecules of type a), Figure 10, also shows improved efficiencies in organic light emitting diodes.[xvi] The improved efficiency is due to better *FF* (63% versus 53%). The mechanism of this observation has not been investigated. It is hypothesized that the insertion of the interfacial dipole lowered the effective work function of the Al cathode. The lower work function cathode increases the offset in potential between the asymmetric electrodes, thereby raising the strength of the built-in electric field. This increased electric field facilitated the transport of charge carriers to their respective electrodes, lowering the probability of charge recombination and contributing to the significant increase in the *FF*.

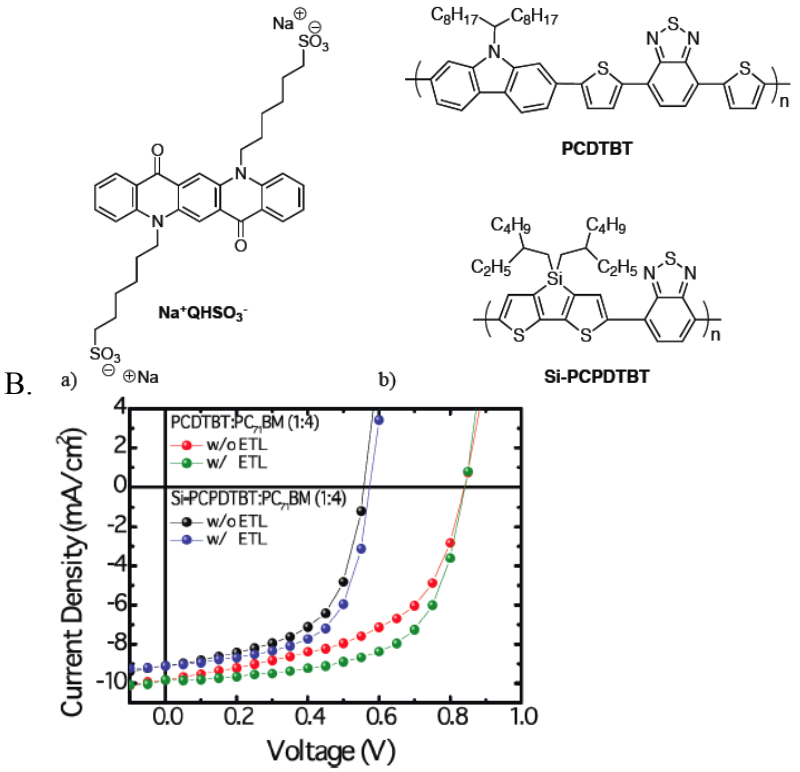

Figure 10. (a) Chemical structure of electron transporting layer. (b) Chemical structures of low band gap conjugated polymers used as donors in BHJ solar cells. (c) Device performance of solar cells with and without the $Na^+QHSO_3^-$-based ETL.

The small molecule oligoelectrolyte shown in Figure 10 is based on a very inexpensive commercially available molecule.[xvii] Many derivatives bearing negative as well as positive termini will be synthesized by simple 1- and two-step processes.

5. Conclusions

The development of stable third-generation polymeric materials for photovoltaic applications has enabled detailed study into the charge transfer and recombination dynamics that produce efficient polymer BHJ solar cells

Publications 2009 - 2011

Bulk heterojunction solar cells with internal quantum efficiency approaching 100%, S. H. Park, A. Roy, S. Beaupre´, S. Cho, N. Coates, J. S. Moon, D. Moses, M. Leclerc, K. Lee, A. J. Heeger, Nature Photonics 3 297 (2009).

Influence of Alkyl Substituents and Thermal Annealing on the Performance Solution Processed, Diketopyrrolopyrrole-Based Bulk Heterojunction Solar Cells, A. Tamayo, T. Kent, T.-Q. Nguyen, Energy Environ. Sci., 2009, 2, 1180-1186

Efficiency Enhancement in Low-Bandgap Polymer Solar Cells by Processing with Alkane Dithiols, Peet, J.; Kim, J.Y.; Coates, N.E.; Ma, W.L.; Moses, D.; Heeger, A.J.; Bazan, G.C., *Nat. Mat.*, 2007, *7*, 497-500.

Improved Performance of Polymer Bulk Heterojunction Solar Cells Through the Reduction of Phase Separation via Solvent Additives, C. V. Hoven; X.D. Dang; R.C. Coffin; J. Peet,; T-Q. Nguyen; G.C. Bazan, *Adv. Mat.*, 2010, *22*, E63-E66.

Streamlined Microwave-Assisted Preparation of Narrow-Bandgap Conjugated Polymers for High-Performance Bulk Heterojunction Solar Cells, Coffin, R.C.; Peet, J.; Rogers, J.; Bazan, G.C., *Nat. Chem.*, 2009, *1*, 657-661.

Higher Molecular Weight Leads to Improved Photoresponsivity, Charge Transport and Interfacial Ordering in a Narrow Bandgap Semiconducting Polymer, M. Tong, S. Cho, J. T. Rogers, K. Schmidt, B. B. Y. Hsu, D. Moses, R. C. Coffin, E. J. Kramer, G. C. Bazan, A. J. Heeger, Adv. Funct. Mater. 20, 3959–3965 (2010).

Bulk Heterojunction Solar Cells with Large Open-Circuit Voltage: Electron Transfer with Small Donor-Acceptor Energy Offset, X. Gong, M. Tong, F. G. Brunetti, J. Seo, Y. Sun, D. Moses, F. Wudl, A. J. Heeger, Adv. Mater., 23, 2272–2277 (2011).

A study of stabilization of P3HT/PCBM organic solar cells by photochemical active TiOx layer, J. Li, S. Kim, S. Edington, J. Nedy, S. Cho, K. Lee, A. J. Heeger, M. C. Gupta, J. T. Yates Jr., Solar Energy Materials & Solar Cells 95 1123–1130 (2011).

Interface state recombination in organic solar cells, R. A. Street, M. Schoendorf, A. Roy, J. H. Lee, Phys. Rev. B 81, 205307 (2010).

Recombination in polymer-fullerene bulk heterojunction solar cells, S. R. Cowan, A. Roy, A. J. Heeger, Phys. Rev. B 82, 245207 (2010).

Effect of Charge Recombination on the Fill Factor of Small Molecule Bulk Heterojunction Solar Cells, Yuan Zhang, Xuan-Dung Dang, Chunki Kim, and Thuc-Quyen Nguyen, Adv. Energy Mater. 1: 610–617 (2011).

Sequential Processing: Control of Nanomorphology in Bulk Heterojunction Solar Cells, D. H. Wang, J. S. Moon, J. Seifter, J. Jo, J. H. Park, O. O. Park, A. J. Heeger, Nano Lett. 11 (8), 3163-3168 (2011).

Ultrafast Relaxation of the P3HT Emission Spectrum, N. Banerji, S. Cowan, E. Vauthey, A. J. Heeger, J. Phys. Chem. C 115, 9726–9739 (2011).

Enhanced Power Conversion Efficiency in Silver Clusters Embedded PCDTBT/$PC_{70}BM$ Bulk Heterojunction Photovoltaic Devices, D. H. Wang, K. H. Park, J. H. Seo, J. Seifter, S. H. Im, J. H. Park, O. O. Park, A. J. Heeger, Adv. Energy Mater., 1(5), 766-770 (2011).

Improved High Efficiency Organic Solar Cells via Incorporation of a Conjugated Polyelectrolyte Interlayer, J. H. Seo, A. Gutacker, Y. Sun, H. Wu, F. Huang, Y. Cao, U. Scherf, A. J. Heeger, G. C. Bazan, J. Am. Chem. Soc., 133, 8416–8419 (2011).

Identifying a threshold impurity level for organic solar cells: Enhanced first-order recombination via well-defined $PC_{84}BM$ traps in organic bulk heterojunction solar cells, S. R. Cowan, W. L. Leong, N. Banerji, G. Dennler, A. J. Heeger, Adv. Funct. Mater. 21: 3083–3092 (2011).

Synthesis and Characterization of 2,8-Diazaperylene-1,3,7,9-tetraone, a New Anthracene Diimide Containing Six-Membered Imide Rings, Ail Reza Mohebbi, Cedric Miñoz and Fred Wudl, Organic Letters 2011 13 (10), 2560-2563

"Nanostructure and optoelectronic characterization of small molecule bulk heterojunction solar cells by photoconductive atomic force microscopy," X.-D. Dang, A. Tamayo, J. Seo, C. Hoven, B. Walker, T.-Q. Nguyen, Adv. Func. Mater. 20, 3314–3321 (2010).

"Exciton Formation, Relaxation, and Decay in PCDTBT," N. Banerji, S. Cowan, M. Leclerc, E. Vauthey, A. J. Heeger, J. Am. Chem. Soc. 132, 17459–17470 (2010).

Higher Molecular Weight Leads to Improved Photoresponsivity, Charge Transport and Interfacial Ordering in a Narrow Bandgap Semiconducting Polymer, M. Tong , S. Cho , J. T. Rogers , K. Schmidt , B. B. Y. Hsu , D. Moses , R. C. Coffin , E. J. Kramer , G. C. Bazan , A. J. Heeger, Adv. Funct. Mater., 20, 3959–3965 (2010).

Solution-processed cross-linkable hole selective layer for polymer solar cells in the inverted structure, Y. Sun, X. Gong, B. B. Y. Hsu, H-L. Yip, A. K.-Y. Jen, A. J. Heeger, Appl. Phys. Lett. 97, 193310 (2010).

Photocarrier relaxation through the manifold of localized states in a polymer-fullerene bulk heterojunction material, N. E. Coates, D. Moses, A. J. Heeger, Appl. Phys. Lett. 98, 10, 102103 (2011).

Enhancement of power conversion efficiency from Au nanoparticles in donor-acceptor polymer bulk-heterojunction solar cells, D. H. Wang, D. Y. Kim, K. W. Choi, J. H. Seo, S. H. Im, J. H. Park, O. O. Park, A. J. Heeger, Angew. Chem., Int. Ed., 50, 1-6 (2011).

Spontaneous Formation of Bulk Heterojunction Nanostructures: Multiple Routes to Equivalent Morphologies, J. S. Moon, C. J. Takacs, Y. Sun, A. J. Heeger, Nano Lett., 11, 1036–1039 (2011).

C. Period 2012 – 2014

a) Charge transfer and photogeneration of mobile charge carriers***:*** Coherence and Uncertainty in Nanostructured Materials

Following the discovery of ultrafast charge transfer in the Heeger Group in 1992, the nano-organic (bulk heterojunction, BHJ) concept was formulated. The need for a morphology comprising two interpenetrating bicontinuous networks was clear: one network to carry the photogenerated electrons to the cathode and one network to carry the holes to the anode. This morphology has now been clearly established using TEM either in the Phase Contrast mode or via TEM-Tomography.

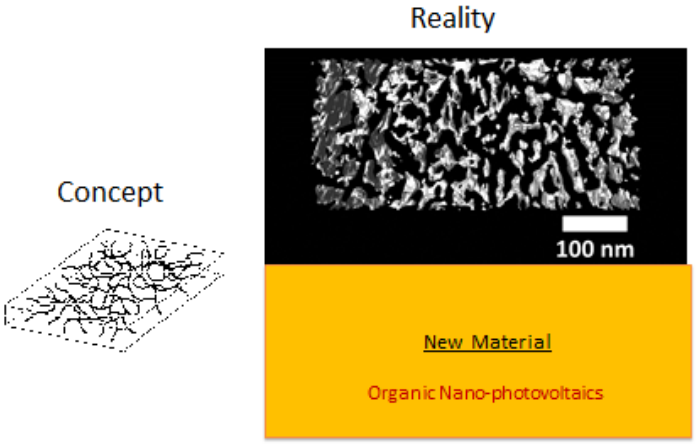

Figure1: Comparison between "concept" and reality in BHJ materials.

The steps involved in delivering power to an external curcuit are listed below:

1. **Photo-excitation of the donor (or the acceptor).**
2. **Charge tranfser with holes in the donor domain and electrons in the acceptor domain.**
3. **Sweep-out to electrodes prior to recombination by the internal electric field.**
4. **Energy delivered to the external circuit**

Figure 2 shows the normalized intensity of the transient absorption signal associated with carriers produced as a result of charge transfer, plotted as a function of time delay between pump and probe pulses. The dynamics display universal behavior, independent of the materials, and correspondingly, independent of the fine details of sample morphology. The data are characterized by a component which rises on a timescale less than 100 fs and a second, slower component which rises on a timescale of approximately 50 ps. The number of charges generated by the ultrafast mechanism saturates after 100 fs; the mechasnism terminates at this extremely short time scale.

Given the disordered, phase separated nano-structure shown in Figure 1, the fundamental question is obvious.How is this ultrafast charge transfer over such large distances in times less than 50 ps possible?

In organic photovoltaic devices, the role of coherence in the charge generation processes has been underexplored, despite the fact that coherent phenomena have been observed in solution phase photon echo measurements of the exact donor materials that are used in bulk heterojunction blends. [(a) Collini et al *Science* **323**, 369-373, (2009). (b) Yang et al S *Physical Review B* **71**, 045203, (2005). (c) Wells, N. P. & Blank, D. A. *Phys. Rev. Lett.* **100**, 08640, (2008)]. These observations require a re-examination of the prevailing organic photovoltaic dogma which states that light absorption creates (at all timescales > 1 fs) a localized exciton which hops randomly and incoherently before encountering an interface at which charge transfer and charge separation occurs [Clarke, T. M. & Durrant, J. R. *Chemical Reviews* 110, 6736-677, (2010)].

As a result of the Uncertainty Principle, the wave function of the photoexcited state of a BHJ material is a delocalized coherent superposition of the eigenfunctions of the Schroedinger equation that describe the nanostructured organic photovoltaic blend. Prior to the collapse of the initially delocalized coherent state there is an ***immediate probability*** of finding an excitation at an interface of a donor-acceptor heterojunction leading to ultrafast electron transfer (fs regime) over relatively long distances.

Photon momentum is uncertain during the absorption process, requiring that its position, as well as the position of the photoexcitation it creates is uncertain, as required by the Heisenberg inequality: $\Delta x\, \Delta p \geq \frac{\hbar}{2}$. The length scale imposed by the Uncertainty Principle is $\lambda/4\pi$, which is greater than 20 nm for visible radiation. As a result, a coherent superposition of the the eigenfunctions of the Schroedinger equation that describes the nanostructured organic photovoltaic blend are simultaneously excited during the photon absorption process.

Fig. 2 shows the normalized intensity of the transient absorption signal associated with carriers produced as a result of charge transfer, plotted as a function of time delay between pump and probe pulses. ***The dynamics display universal behavior, independent of the materials, and correspondingly, independent of details of sample morphology.*** The data indicate component which rises on a timescale less than 100 fs and a second, slower component which rises on a timescale of approximately 50 ps. The ***startling generality*** implies that the lifetime of the delocalized coherent state is sufficiently long that it plays an important role in the charge transfer from donor domains to acceptor domains

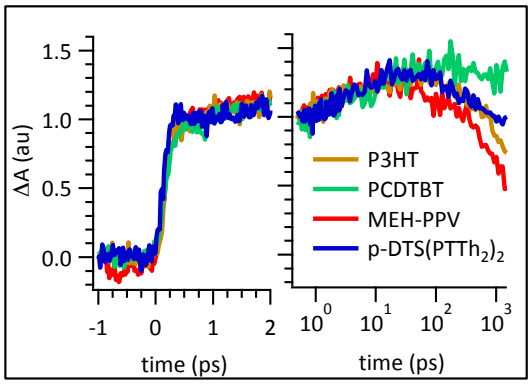

Figure 2: Transient absorption of bulk heterojunction materials.
Left: Integrated spectral intensity associated with mobile carriers, normalized to the intensity at 100 fs and plotted on a linear scale near zero time delay.
Right: Semi-log plot of the integrated spectral intensity associated with the slower component of the mobile carrier generation process, normalized to the intensity at 100 fs. The pump intensity is < 1μJ/cm^2. The ultrafast increase of the charge carrier dynamics in Fig. 2 is known to arise from ultrafast electron transfer between the electron donor and the fullerene acceptor in the nanostructured material. The slower rising component results from exciton diffusion to a heterojunction interface where they are split, forming charge carriers; holes on the donor side of the heterojunction and electrons on the acceptor side. The observed time scale for the increase in carrier density (≈ 50 ps) is consistent (for transport over approx. 10 nm) with known diffusion

These conclusions are supported by measurements of the pump power dependence of the two components (data not shown). The ultrafast component is linear in pump intensity over two orders of magnitude. The exciton component is strongly nonlinear at pump intensities greater than ~10 μJ/ cm^2 as a result of exciton-exciton annihilation and exciton-charge annihilation, which destroy diffusing excitons prior to reaching a charge transfer interface. The ratio between the contributions from ultrafast charge transfer and charge transfer following exciton diffusion is 0.31 ± 0.02. This implies that the coherent state which exists at the shortest timescales interacts with approx. the same volume of material as the subsequently diffusing excitons consistent with the collapse of the coherent delocalized wave function after approx. 1 ps.

Even in solution, coherence in pristine MEH-PPV has been observed to persist to ~25 fs [Yang et al *Physical Review B* 71, 045203, (2005)] and in pristine SP3HT to ~100 fs [Wells et al *Phys. Rev. Lett.*

100, 086403, (2008)] implying that in BHJ phase separated blends, a coherent state exists with sufficient lifetime that it enables the electron transfer/charge separation processes.

In conclusion, transient absorption demonstrated the importance of coherent effects in nano-organic solar cells. The results show generality in the charge generation dynamics of organic BHJ materials that is unexpected. The creation of long range coherent superposition states is a natural consequence of the Uncertainty Principle, as applied to the photon absorption process. We expect that phenomena of this type are important not only for organic bulk heterojunction solar cells, but for nanostructured materials in general.

b) Synthesis of new materials

To improve the interface between the donor polymer and acceptor in BHJ cells and enhance the absorption in the visible-near IR region we designed polymer **2** using our previously designed novel large π-surface emeraldicene (**1**). Indeed the copolymer **2** has an absorption extending all the way to the near IR as shown in the spectrum below.

A surprising result was that this polymer exhibits high and AMBIPOLAR mobilities (as High as0.3 cm^2 $V^{-1}sec^{-1}$) upon annealing to 320˚C.

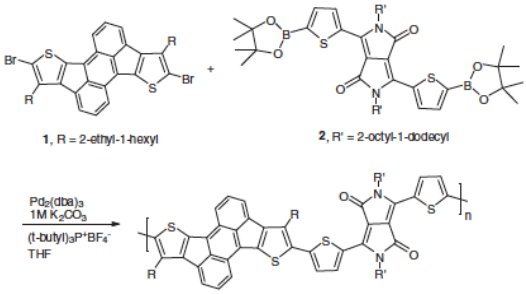

This polymer exhibits relatively high AMBIPOLAR mobilities (as high as 0.3 cm^2 $V^{-1}sec^{-1}$) annealing to 320˚C.

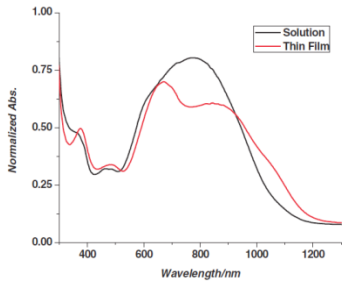

Another polymer that was designed with the same goal in mind is PBBTTT, shown below.

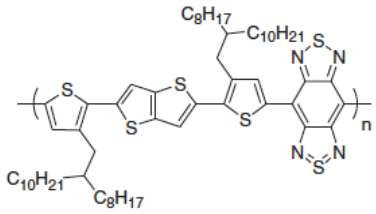

PBBTTT

This polymer also absorbs extensively into the near IR and is an even better charge transport material than polymer **2** (see above for structure), exhibiting ambipolar mobilities on the order of 1 cm^2 $V^{-1}sec^{-1}$ when annealed and crystallized at 320˚C, shown

Another interfacial polymer we prepared is PBBTQT that absorbs all the way into the near IR (1800 nm), crystallizes near 260˚C and shows a high hole mobility of up to 3 $cm^2V^{-1}sec^{-1}$.

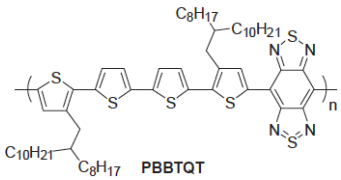

PBBTQT

c) Interfacial Effects in Organic Bulk Heterojunction Solar Cells

Recently, significant efforts have been dedicated to the interface engineering of organic solar cells. Many interfacial materials, such as metal oxides, selfassembled monolayers (SAMs) and conjugated polyelectrolytes (CPEs), have successfully enhanced PCEs of solar cells fabricated through solution processing using orthogonal solvent such as methanol. More interestingly, several independent groups have found that the device performance could be considerably enhanced by treatment with polar solvents that are commonly used in interface engineering through solution processing in organic photovoltaics before deposition of metal electrodes. However, these interesting phenomena and attractive effects originating from simple solvents treatment are poorly understood. This year, we have focused on understanding the effect of solvent treatment on the device physics of polymer BHJ solar cells. Methanol was chosen as typical solvent because it has been widely used in surface engineering to incorporate interlayers in photovoltaics.

Conjugated polyelectrolyte (CPEs) were one of the core subjects of study. CPEs are defined as conjugated polymers bearing pendent ionic groups. The Figure below shows a generic and a specific CPE structure. CPEs are unique materials in that they embody the electronic properties of organic semiconductors with the ability of polyelectrolytes to have their properties and function modulated by electrostatic interactions. A practical consequence of their charged nature is that CPEs are soluble in water or polar organic solvents. Multilayer polymer devices can therefore be easily fabricated by solution-processing methods that alternate solvent polarity, i.e. the orthogonal solvent approach.

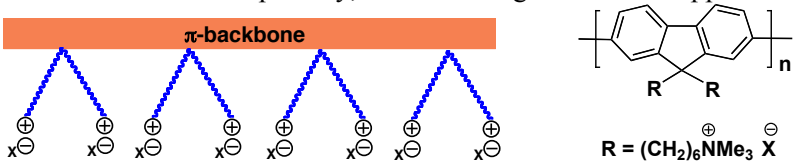

There are two general hypotheses for the working mechanisms in devices utilizing CPEs: the formation of an aligned interfacial dipole layer (thin CPE layers) and ion motion followed by electrostatic field redistribution (thicker CPE layers). The dipole-mediated mechanism is conceptually simpler and is discussed first. Note that the first scenario is based on charge tunneling and thus necessarily requires the layer to be thin. While this aligned dipole mechanism is widely accepted in the literature, there is virtually no information on what prevents electrostatic dipoles to pair up and thereby yield a net neutral surface. A related question is the fraction of dipoles actually formed per unit area.

The UCSB team provided the mechanistic basis for operation of thicker CPE layers in OLEDs, as illustrated in the Figure below for the case of an ITO/PEDOT:PSS/MEH-PPV/CPE/Al device with 5V applied bias. The CPE used here is **PFN-BIm$_4$** (see Figure for chemical structures). MEH-PPV here serves as the electroluminescent layer. PEDOT:PSS is the widely used hole injection layer poly(3,4-ethylenedioxythiophene):poly(styrenesulfonicacid). As holes are injected, they accumulate at the MEH-PPV/CPE interface and screen the electric field in the MEH-PPV layer, as shown in the transition from (a) to (b) in the figure below. The electric field is thereby redistributed so that voltage drops

predominantly across the CPE producing a large internal field within that layer. This large internal field leads to anion motion toward the MEH-PPV/CPE interface, leaving an excess of cations adjacent to the cathode. The electric field across the CPE is therefore redistributed into two double layers at the MEH-PPV/CPE interface and at the CPE/cathode interface, as in (c). The end result is that the electric fields in both layers are screened with nearly all of the applied voltage localized across the double layers. Consequently, although the electron injection barrier (φ) remains the same, efficient electron injection occurs via tunneling through the ultra-thin double layer and radiative recombination of electrons and holes occurs in the MEH-PPV near the CPE interface. Because the internal electric field is screened and nearly zero in both layers, the hole and electron currents are diffusion currents rather than drift currents.

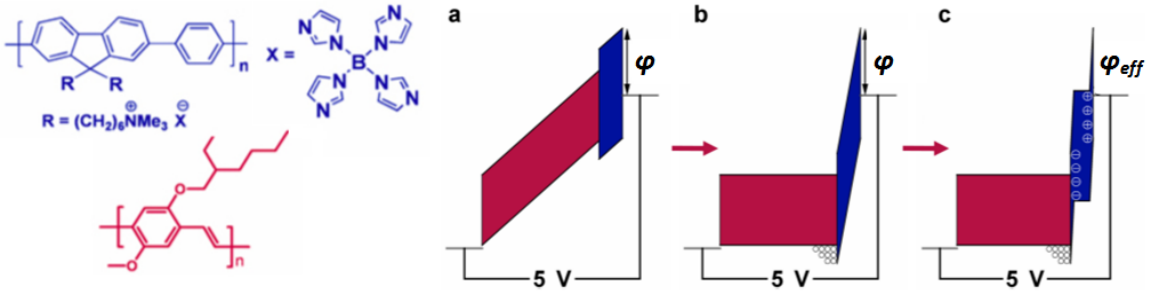

Molecular structures of **PFN-BIm$_4$** (blue) and MEH-PPV (red). Schematic response of an ITO/PEDOT:PSS/MEH-PPV/**PFN-BIm$_4$**/Al device under 5V applied bias. (a) The electric field (proportional to the slope of the energy levels) is evenly distributed across the device. (b) Holes (empty circles) accumulate at the MEH-PPV/**PFN-BIm$_4$** interface, screening the electric field to the **PFN-BIm$_4$** layer. (c) Ions then redistribute to screen the electric field to the MEH-PPV/ **PFN-BIm$_4$** and **PFN-BIm$_4$**/Al interfaces.

These concepts were productively introduced into the BHJ solar cell research. As an example, see the figure below which demonstrates a significant enhancement in power conversion efficiency.

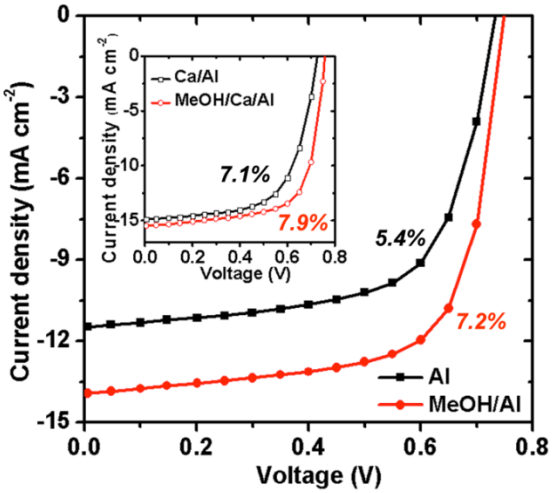

Current density-voltage characteristics of devices: ITO/PEDOT:PSS/ PTB7:PC$_{70}$BM/Al or Ca/Al cathodes where the active layer was treated with methanol (MeOH). The reference devices without MeOH treatment were included for comparison.

The power conversion efficiency can be improved in thieno[3,4-b]-thiophene/benzodithiophene:[6,6]-phenyl C71-butyric acid methyl ester (PTB7:PC$_{70}$BM) solar cells by methanol treatment from 7.1% to 7.9% when Ca/Al is used as cathodes, while from 5.4% to 7.2% using Al as cathodes (Figure 5). Kelvin probe force microscopy, XPS, charge transport, impedance spectra, and

transient photoconductivity measurements have been used to study this phenomenon. KPFM measurements of the surface of the active layer show a 101 ± 19 mV shift in average surface potential occurring after methanol treatment, which suggests that at the metal/organic interface, the vacuum level (VL) of the cathode is correspondingly elevated 101 ± 19 mV simply by methanol treatment. The surface potential is an extremely sensitive indicator of surface condition and can be affected by electronic states on the surface including surface charge density or surface traps, surface reconstruction, and chemical composition, etc. Methanol treatment causes no obvious change on film morphology and surface roughness or film thickness. These observations indicate no evident reconstruction of the surface of PTB7:$PC_{70}BM$ blends after methanol treatment. Thus, the increase of surface potential might originate from the charge of surface electronic states including the diminishment of surface traps or variation of charge density after methanol treatment. Results from this combination experiments suggest that methanol treatment leads to an improvement of built-in voltage, a decrease in series resistance, an enhancement in charge-transport, an accelerated and enhanced charge extraction, and reduced recombination, the combination of which induces a simultaneous enhancement in open-circuit voltage (Voc), short-circuit current (Jsc), and fill factor (FF) in the devices. This result provides deeper insight to understand the mechanism of surface engineering by solution processing which cannot exclude the effect of solvents.

The effect of MeOH treatment is also observed in solution-processed small molecule BHJ solar cells (Figure below). The device characteristics: J_{sc}, V_{oc}, FF, PCE calculated from the J-V curves for all devices are summarized in Table 1. The addition of a PFN-BIm4 interlayer resulted in an increase in V_{oc} from 720 mV to 800 mV, in J_{sc} from 11.3 mA/cm^2 to 12.1 mA/cm^2, and in FF from 57% to 71%, yielding an increase in PCE from 4.6% to 6.8%. Additionally we observed an increase in device characteristics with the methanol control device. While the performance enhancement with methanol was not as great as with the CPE, we note that the increase in J_{sc} and V_{oc} are similar to that with the CPE interlayer; however, the CPE interlayer offers a larger increase in fill factor than the methanol control. These findings are consistent with a multi-faceted mechanism for improvement of power conversion efficiencies involving both the polar solvent and CPE.

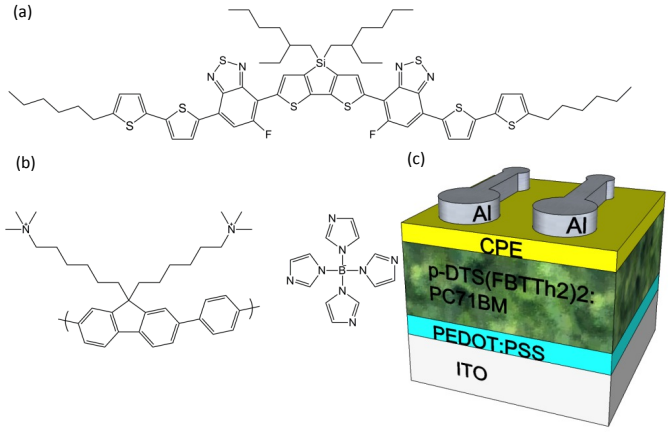

Chemical structures of (a) p-DTS($FBTTh_2$)$_2$, (b) PFN-BIm4 and (c) non-standard device architecture employed.(a) Light and (b) dark J-V curves for CPE and non CPE containing devices.

Table 1. Average device characteristics as well as the "champion" device PCE.

Device	J_{sc} (mA·cm^{-2})	V_{oc} (mV)	FF	PCE	"Champion" PCE	Series Resistance	Shunt Resistance
w/o CPE	-11.3±0.1	710±1	57%±1%	4.6%±0.2%	4.8%	1.52	41094
w/ methanol	-11.9±0.5	780±2	64%±2%	6.0%±0.3%	6.4%	3.08	10001
w/PFN-BIm4	-12.1±0.2	800±2	71%±1%	6.8%±0.2%	7.0%	1.82	100386

4. Publications (with Acknowledgement to DE-FG02-08ER46535)

1. Transient Photocurrent Response of Small-Molecule *Bulk Heterojunction Solar Cells*, Jason Seifter, Yanming Sun, and Alan J. Heeger, Adv. Mater., 26, 2486 (2014).

2. Role of Localized States on Carrier Transport in Bulk Heterojunction Materials Comprised of Organic Small Molecule Donors, C. Zhong, F. Huang, Y. Cao, D. Moses, and Alan J. Heeger, *Adv. Mater.* Volume 26, , 2341, April 16, 2014

2. Single-Crystal Linear Polymers Through Visible Light-Triggered Topochemical Quantitative Polymerization, L.T. Dou, Y. H. Zheng, X. Q. Shen, G. Wu, K. Fields, W. C. Hsu, H. P. Zhou, Y. Yang, and F. Wudl, *Science* **2014**, *343*, 272.

3. Organic spin transporting materials: present and future, Y. H. Zheng, and F. Wudl, *J. Mater. Chem. A* **2014**, *2*, 48.

4. Facile Doping of Anionic Narrow-Band-Gap Conjugated Polyelectrolytes During Dialysis, C. K. Mai, H. Q. Zhou, Y. Zhang, Z. B. Henson, T.-Q. Nguyen, A. J. Heeger, and G. C. Bazan, *Angew. Chem. Int. Ed.* **2013**, *52*, 12874.

5. "Tri-Diketopyrrolopyrrole Molecular Donor Materials for High-Performance Solution-Processed Bulk Heterojunction Solar Cells", J. H. Liu, Y. M. Sun, P. Moonsin, M. Kuik, C. M. Proctor, J. S. Lin, B. B. Hsu, V. Promarak, A. J. Heeger, and T.-Q. Nguyen, *Adv. Mater.* **2013**, *25*, 5898.

6. Barium: An Efficient Cathode Layer for Bulk-Heterojunction Solar Cells, V. Gupta, A. K. K. Kyaw, D. H. Wang, S. Chand, G. C. Bazan, and A. J. Heeger, *Sci. Rep.* **2013**, *3*, 1965.

7. Intensity Dependence of Current-Voltage Characteristics and Recombination in High-Efficiency Solution-Processed Small-Molecule Solar Cells, A. K. K. Kyaw, D. H. Wang, V. Gupta, W. L. Leong, L. Ke, G. C. Bazan, and A. J. Heeger, *ACS Nano* **2013**, *7*, 4569.

8. Fullerene concentration dependent bimolecular recombination in organic photovoltaic films, L. G. Kaake, Y. M. Sun, G. C. Bazan, and A. J. Heeger, *Appl. Phys. Lett.* **2013**, *102*, 133302.

9. High-Efficiency Polymer Solar Cells Enhanced by Solvent Treatment, H. Q. Zhou, Y. Zhang, J. Seifter, S. D. Collins, C. Luo, G. C. Bazan, T.-Q. Nguyen, and A. J. Heeger, *Adv. Mater.* **2013**, *25*, 1646.

10. High-Hole-Mobility Field-Effect Transistors Based on Co-Benzobisthiadiazole-Quaterthiophene,,

J. Fan, J. D. Yuen, W. B. Cui, J. Seifter, A. R. Mohebbi, M. F. Wang, H. Q. Zhou, A. Heeger, and F. Wudl, *Adv. Mater.* **2012**, *24*, 6164.

11. Insights into pi-Conjugated Small Molecule Neat Films and Blends As Determined Through Photoconductivity, J. J. Jasieniak, B. B. Y. Hsu, C. J. Takacs, G. C. Welch, G. C. Bazan, D. Moses, and A. J. Heeger, *ACS Nano* **2012**, *6*, 8735.

12. A Solution-Processed MoO_x Anode Interlayer for Use within Organic Photovoltaic Devices, J. J. Jasieniak, J. Seifter, J. Jo, T. Mates, and A. J. Heeger, *Adv. Funct. Mater.* **2012**, *22*, 2594.

13. Breaking Down the Problem: Optical Transitions, Electronic Structure, and Photoconductivity in Conjugated Polymer PCDTBT and in Its Separate Building Blocks, N. Banerji, E. Gagnon, P. Y. Morgantin, S. Valouch, A. R. Mohebbi, J. H. Seo, M. Leclerc, and A. J. Heeger, *J. Phys. Chem. C* **2012**, *116*, 11456.

14. Single Nanowire OPV Properties of a Fullerene-Capped P3HT Dyad Investigated Using Conductive and Photoconductive AFM, D. A. Kamkar, M. F. Wang, F. Wudl, and T.-Q. Nguyen, *ACS Nano* **2012**, *6*, 1149.

15. Ribbons, Vesicles, and Baskets: Supramolecular Assembly of a Coil-Plate-Coil Emeraldicene Derivative, W. F. Wang, A. R. Mohebbi, Y. M. Sun, and F. Wudl, *Angew. Chem. Int. Ed.* **2012**, *51*, 6920.

16. Emeraldicene as an Acceptor Moiety: Balanced-Mobility, Ambipolar, Organic Thin-Film Transistors, A. R. Mohebbi, J. Yuen, J. Fan, C. Munoz, M. F. Wang, R. S. Shirazi, J. Seifter, and F. Wudl, *Adv. Mater.* **2011**, *23*, 4644.

17. Exciton Formation, Relaxation, and Decay in PCDTBT, N. Banerji, S. Cowan, M. Leclerc, E. Vauthey, A. J. Heeger, J. Am. Chem. Soc., **2010**, 132, 17459.

18. Solution-processed cross-linkable hole selective layer for polymer solar cells in the inverted structure, Y. Sun, X. Gong, B. B. Y. Hsu, H-L. Yip, A. K.-Y. Jen, A. J. Heeger, Appl. Phys. Lett. **2010**, 97, 193310.

19. Photocarrier relaxation through the manifold of localized states in a polymer-fullerene bulk heterojunction material, N. E. Coates, D. Moses, A. J. Heeger, Appl. Phys. Lett. **2011**, 98, 10, 102103.

20. Ultrafast Relaxation of the Poly(3-hexylthiophene) Emission Spectrum, N. Banerji, S. Cowan, E. Vauthey, A. J. Heeger, J. Phys. Chem. C, **2011**, 115, 9726.

21. Enhancement of Donor-Acceptor Polymer Bulk Heterojunction Solar Cell Power Conversion Efficiencies by Addition of Au Nanoparticles, D. H. Wang, D. Y. Kim, K. W. Choi, J. H. Seo, S. H. Im, J. H. Park, O. O. Park, A. J. Heeger, Angew. Chem. Int. Ed., **2011**, 50, 24, 5519.

22. Enhanced Power Conversion Efficiency in PCDTBT/PC(70)BM Bulk Heterojunction Photovoltaic Devices with Embedded Silver Nanoparticle Clusters, D. H. Wang, K. H. Park, J. H. Seo, J. Seifter, J. H. Jeon, J. K. Kim, J. H. Park, O. O. Park, A. J. Heeger, Adv. Energy Mater., **2011**, 1(5), 766.

23. Spontaneous Formation of Bulk Heterojunction Nanostructures: Multiple Routes to Equivalent Morphologies, J. S. Moon, C. J. Takacs, Y. Sun, A. J. Heeger, Nano Lett., **2011**, 11, 1036.

24. Bulk Heterojunction Solar Cells with Large Open-Circuit Voltage: Electron Transfer with Small Donor-Acceptor Energy Offset, X. Gong, M. Tong, F. G. Brunetti, J. Seo, Y. Sun, D. Moses, F. Wudl, A. J. Heeger, Adv. Mater., **2011**, 23, 2272.

25. Improved High-Efficiency Organic Solar Cells via Incorporation of a Conjugated Polyelectrolyte Interlayer, J. H. Seo, A. Gutacker, Y. Sun, H. Wu, F. Huang, Y. Cao, U. Scherf, A. J. Heeger, G. C. Bazan, J. Am. Chem. Soc., **2011**, 133, 8416.

26. Identifying a Threshold Impurity Level for Organic Solar Cells: Enhanced First-Order Recombination Via Well-Defined $PC_{84}BM$ Traps in Organic Bulk Heterojunction Solar Cells, S. R. Cowan, W. L. Leong, N. Banerji, G. Dennler, A. J. Heeger, Adv. Funct. Mater., **2011**, 21, 3083.

27. Sequential Processing: Control of Nanomorphology in Bulk Heterojunction Solar Cells, D. H. Wang, J. S. Moon, J. Seifter, J. Jo, J. H. Park, O. O. Park, A. J. Heeger, Nano Lett. **2011**, 11, 3163.

28. Ultrafast spectroscopic investigation of a fullerene poly(3-hexylthiophene) dyad, N. Banerji, J. Seifter, M. Wang, E. Vauthey, F. Wudl, A. J. Heeger, Phys. Rev. B **2011**, 84, 075206.

29. Manifestation of carrier relaxation through the manifold of localized states in PCDTBT:PC70BM bulk heterojunction material: The role of PC84BM traps on the carrier transport; Wei Lin Leong, Gerardo Hernandez-Sosa, Sarah R. Cowan, Daniel Moses, and Alan J. Heeger; Adv. Mater. **2012**, 24, 2273

30. Charge Formation, Recombination and Sweep-out Dynamics in Organic Solar Cells; Sarah R. Cowan, Natalie Banerji, Wei Lin Leong, and Alan J. Heeger; Feature Article in Adv. Funct. Mater.**2012**, 22, 1116.

31. Role of Localized States on Carrier Transport in Bulk Heterojunction Materials Comprised of Organic Small Molecule Donors, C. Zhong, F. Huang, Y. Cao, D. Moses, and Alan J. Heeger, Adv. Mater. **2014**, 26, 2341.

32. Effect of Molecular Order on the Performance of Naphthobisthiadiazole-Based Polymer Solar Cells, Y. Sun, J. Seifter, M. Wang, L. A. Perez, C. Luo, G. C. Bazan, F. Huang, Y. Cao, A. J. Heeger, Adv. Energy Mater., **2014**, 4, 1301601.

33. Design and Properties of Intermediate-Sized Narrow Band-Gap Conjugated Molecules Relevant to Solution-Processed Organic Solar Cells, X. Liu, Y. Sun, B. B. Y. Hsu, A. Lorbach, L. Qi, A. J. Heeger, G. C. Bazan, J. Am. Chem. Soc. **2014**, 136 (15), 5697.

34. Transient Photocurrent Response of Small-Molecule Bulk Heterojunction Solar Cells, J. Seifter, Y. Sun, A. J. Heeger, Adv. Mater., **2014**, 26, 2486.

35. Effects of Solvent Additives on Morphology, Charge Generation, Transport, and Recombination in Solution Processed Small-Molecule Solar Cells, A. K. K. Kyaw, D. H. Wang, C. Luo, Y. Cao, T. Q. Nguyen, G. C. Bazan, A. J. Heeger, Adv. Energy Mater.,**2014**, 4, 1301469.

36. Bulk Heterojunction Solar Cells: Morphology and Performance Relationships, Y. Huang, E. J. Kramer, A. J. Heeger, G. C. Bazan, Chem. Rev. **2014**, 114 (14), 7006-7043.

37. A Stable Polyaniline-Benzoquinone-Hydroquinone Supercapacitor, D. Vonlanthen, P. Lazarev, K. A. See, F. Wudl, A. J. Heeger, Adv. Mater.,**2014**, 26, 5095.

38. Conductive Conjugated Polyelectrolyte as Hole Transporting Layer for Organic Bulk Heterojunction Solar Cells, Huiqiong Zhou, Yuan Zhang, Cheng-Kang Mai, Samuel D. Collins, Thuc-Quyen Nguyen, Guillermo C. Bazan, Alan J. Heeger, Adv. Mater. **2014**, 26, 780.

39. Electronic Properties of Conjugated Polyelectrolyte/Single Walled Carbon Nanotube Composites, Yao Li, Cheng-Kang Mai, Hung Phan, Xiaofeng Liu, Thuc-Quyen Nguyen, Guillermo C. Bazan , Mary B. Chan-Park, Adv. Mater. **2014**, 26, 4697.

40. Striking Effect of Intra- versus Intermolecular Hydrogen Bonding on Zwitterions: Physical and Electronic Properties, Yonghao Zheng, Mao-sheng Miao, Yuan Zhang, Thuc-Quyen Nguyen, and Fred Wudl, Journal of the American Chemical Society **2014** 136 (33), 11614.

The four PI's presented invited lectures at scientific conferences all over the world, many of them were Plenary Lectures. There are no published Conference Proceedings.

5. Web site or other Internet sites that reflect the results of this project
None

6. Networks or collaborations fostered

a. Professor Yong Cao and colleagues at the South China Institute of Technology (SCUT), Guangzhou, China
Exchange meetings were held every year with a group of students and post-docs going from UCSB to SCUT (or vice versa)

b. Group interactions with Prof. Jean-Luc Bredas, Prof. Seth Marder and Prof. Bernard Kippelen are ongoing This interaction subsequently resulted in the funding by the Office of Naval Research of a five-year Multi-University Research Initiative (MURI) focused on the science of plastic solar cells (Bulk Heterojunction Solar cells).

7. Technologies/Techniques

Major demonstration projects directed toward commercialization of BHJ solar cells were carried out by Konarka Technologies. Some examples are shown in the images below:

Plastic Solar Cells

Nano-OPV

Roll-to-Roll manufacturing in large scale

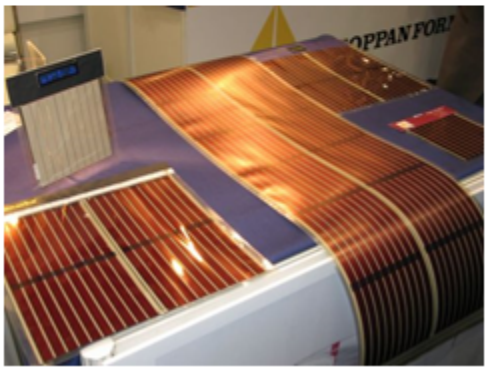

Konarka Inc. was successful in demonstrating the feasibility of large scale roll-to-role manufacturing by solution based printing technology. They were, however too early --- the power conversion efficiencies were not yet sufficiently high to enable the development of a significant market. The company went into bankruptcy in 2011. These demonstration projects were important in that they clearly demonstrated the reality of the potential opportunity for plastic solar cells.

8. Inventions/Patent Applications

"Multicomponent Polymer Supercapacitor with Enhanced Stability and Capacitance"
Authors: Heeger, Alan J.; Vonlanthen, David; Wudl, Fred
Docket No.: 2013-752 (patent pending)

9. Other products

Results from this grant were incorporated into teaching undergraduate and graduate students through a series of graduate level courses at UC Santa Barbara.

---

[i] Banerji, N., Cowan, S., Leclerc, M., Vauthey, E. & Heeger, A. J. Exciton Formation, Relaxation, and Decay in PCDTBT. *J. Am. Chem. Soc.***132**, 17459-17470 (2010).

[ii] Street, R. A., Cowan, S. & Heeger, A. J. Experimental test for geminate recombination applied to organic solar cells. *Phys. Rev. B* **82**, 121301 (2010).

[iii] (a) Cowan, S. R., Street, R. A., Cho, S. & Heeger, A. J. Transient photoconductivity in polymer bulk heterojunction solar cells: Competition between sweep-out and recombination. *Phys. Rev. B* **83**, 035205 (2011). (b) Street, R., Song, K. W., Northrup, J. & Cowan, S. Photoconductivity measurements of the electronic structure of organic solar cells. *Phys. Rev. B* 83, 165207 (2011).

[iv] Cowan, S. R., Roy, A. & Heeger, A. J. Recombination in polymer-fullerene bulk heterojunction solar cells. *Phys. Rev. B* **82**, 245207 (2010).

[vi] (a) G. G. Belmonte, P. P. Boix, J. Bisquert, M. Sessolo, H. J. Bolink, Simultaneous determination of carrier lifetime and electron density-of-states in P3HT:PCBM organic solar cells under illumination by impedance spectroscopy. *Sol. Energ. Mat. Sol. C* **94**, 366 (2010). (b) Yuan Zhang, Xuan-Dung Dang, Chunki Kim, and Thuc-Quyen Nguyen, Effect of Charge Recombination on the Fill Factor of Small Molecule Bulk Heterojunction Solar Cells. *Adv. Energy Mater.,* 1: 610–617. (2011).

[vii] He, C.; Zhong, C.; Wu, H.; Yang, R.; Yang, W.; Huang, F.; Bazan, G. C.; Cao, Y. *J.* Origin of the enhanced open-circuit voltage in polymer solar cells via interfacial modification using conjugated polyelectrolytes. *Mater. Chem.* **20**, 2617 (2010).

[viii] Jiang, H.; Taranekar, P.; Reynolds, J. R.; Schanze, K. S., Conjugated Polyelectrolytes: Synthesis, Photophysics, and Applications. *Angew. Chem. Int. Ed.* **48**, 4300-4316 (2009).

[ix] Barrat, J. L.; Joanny, J. F. Theory of Polyelectrolyte Solutions. *Advances in Chem. Phys.* **94**, 1-66 (1996).

[x] (a) D. W. Steuerman, A. Garcia, R. Yang, and T.-Q. Nguyen, Imaging of Interfaces in Conjugated Polymer Optoelectronic Devices. *Adv. Mater.* **20**, 528-534 (2008). (b) H. Ade, C. Wang, A. Garcia, A. Hexemer, K. E. Sohn, T.-Q. Nguyen, G. C. Bazan, and E. J. Kramer, Characterization of Multicomponent Polymer Trilayers with Resonant Soft X-ray Reflectivity. *Journal of Polymer Science Part B: Polymer Physics* **47**, 1291-1299 (2009). (c) C. Wang, A. Garcia, H. Yan, K. E. Sohn, A. Hexemer, T.-Q. Nguyen, G. C. Bazan, E. J. Kramer, H. Ade, Interfacial widths of conjugated polymer bilayers. *J. Am. Chem. Soc.* **131**, 12538-12539 (2009).

[xi] (a) Hoven, C. V.; Yang, R.; Garcia, A.; Crockett, V.; Heeger, A. J.; Bazan, G. C. Mechanism of electron injection in multilayer polymer light-emitting diodes using conjugated polyelectrolyte as the electron

transporting layer. *Proc. Nat. Acad. Sci. U.S.A.* **105**, 12730 (2008). (b) Bolink, H. J.; Brine, H.; Coronado, E.; Sessolo, M. *ACS Appl. Mater. Interfaces* **2**, 2694 (2010).

[xii] (a) Seo, J. H.; Gutacker, A.; Walker, B.; Cho, S.; Garcia, A.; Yang, R.; Nguyen, T.-Q.; Heeger, A. J.; Bazan, G. C. Improved Injection in n-Type Organic Transistors with Conjugated Polyelectrolytes. *J. Am. Chem. Soc.* **131**, 18220 (2009). (b) Seo, J. H.; Namdas, E. B.; Gutacker, A.; Heeger, A. J.; Bazan, G. C. Conjugated polyelectrolytes for organic light emitting transistors. *Appl. Phys. Lett. 97*, 043303 (2010).

[xiii] Wang, Y.; Liu, B.; Mikhailovsky, A.; Bazan, G. C. Conjugated Polyelectrolyte–Metal Nanoparticle Platforms for Optically Amplified DNA Detection. *Adv. Mater.* **22**, 656 (2010).

[xiv] (a) S. M. Sze, Physics of Semicondutor Devices, 2nd ed., Wiley-Interscience, New York, 1981. (b) C. Waldauf, M. C. Scharber, P. Schilinsky, J. A. Hauch, C. J. Brabec, Physics of organic bulk heterojunction devices for photovoltaic applications. *J. Appl. Phys.* **99**, 104503 (2006).

[xv] Toan V. Pho, Heejoo Kim, Jung Hwa Seo, Alan J. Heeger, and Fred Wudl, Quinacridone-based electron transport layers for enhanced performance in bulkheterojunction solar cells. Adv. Funct. Mater., 21, 4338-4341 (2011).

[xvi] Pho, T. V.; Zalar, P.; Garcia, A.; Nguyen, T.-Q.; Wudl, F. Electron injection barrier reduction for organic light-emitting devices by quinacridone derivatives. *Chemical Communications* **46**, 8210 -12 (2010).

[xvii] Paulus, E.F.; Leusen, F.J.J.; Schmidt, M.U. Crystal Structures of Quinacridones, *Cryst. Eng. Comm.* **9**, 131–143 (2007).